MODELING OF HOPPER DISCHARGE

by

Jiaming Cheng

B.Sc. in Chemical Engineering,

East China University of Science and Technology, 2010

Submitted to the Graduate Faculty of

the Swanson School of Engineering in partial fulfillment

of the requirements for the degree of

Master of Science

University of Pittsburgh

2012

UNIVERSITY OF PITTSBURGH

SWANSON SCHOOL OF ENGINEERING

This thesis was presented

by

Jiaming Cheng

It was defended on

November 2, 2012

and approved by

Joseph J. McCarthy, Professor, Ph.D., Department of Chemical and Petroleum Engineering

Lei Li, Professor, Ph.D., Department of Chemical and Petroleum Engineering

Robert M Enick, Professor, Ph.D., Department of Chemical and Petroleum Engineering

Thesis Advisor: Joseph J. McCarthy, Professor, Ph.D., Department of Chemical and Petroleum Engineering

MODELING OF HOPPER DISCHARGE

Jiaming Cheng, M.S.

University of Pittsburgh, 2012

Hoppers are widely used in many engineering processes. The discharging of granular materials from a hopper is a critical topic of industrial importance, and the discharge flow rate from hoppers is the focus of the current work. Many parameters influence the discharge rate including: the hopper outlet width, the angle of the hopper wall, the particle size, and particle friction, and so on. Due to the expensive of examining a large variety of particle types and hopper conditions, computational simulation has been widely studied in an effort to establish an alternative method of determining critical factors impacting hopper flow.

In this thesis, the process of hopper discharge has been simulated by the Discrete Element Method (DEM), which is one of the most popular methods for granular flow simulation. To validate against existing experiments, all conditions were matched as closely as possible to those in the experiment. The particles used in our simulation are spheroids with diameters of 0.77 cm. The angles of the hoppers examined range from 0° to 90°, while the opening sizes vary from 2.9 cm to 4.3 cm. Computationally, the friction coefficient has been adjusted several times and finally is set to 0.5 in the simulation in order to fit the experimental results as closely as possible. As a quantitative test of the simulation fidelity we compare the hopper

empty time t – which is related to the hopper discharge rate – for these different hopper angles and hopper opening size. As a secondary test of the fit, the survival time τ, the normal force profile, the velocity profile, and the probability of jamming P_s are also computed and compared to existing experimental data from collaborators at Duke University. Ultimately, the goal of the work is to establish the degree of model fidelity necessary in order to closely mimic the experimental results obtained.

Keywords: Granular flow, Hoper discharge, DEM simulation, Probability of jamming

Particle Dynamics (PD), DEM simulation, Granular Media, Granular Flow, Collisional Flow.

TABLE OF CONTENTS

LIST OF FIGURES

NOMENCLATURE

English Symbols:

A	: hopper outlet arear
C	: empirical constant which ranges from 0.55 to 0.65
d_t	: time step
d	: diameter of the particle
d_e	: effective grain particle diameter
dp_j	: probability that a jam occurs in a very short interval
D	: hopper opening size
E^*	: effective Young's modulus
E_i	: Young's modulus
$\vec{F}_n$	: normal force
$\vec{F}_t$	: tangential force
F_y	: yield force
F_{max}	: maximum value of normal force during collision
F_{t0}	: old tangential force
j	: mass flux
k	: Beverloo material dependent constant

k_n : normal contact stiffness

k_y : plastic stiffness

k_t : tangential contact stiffness

k_{t0} : tangential contact stiffness assumed as a content

p_j : probability that the jam happens

p_u : probability that particle system flows fluency without a jam

$P_s(t)$: probability that a flow has survived for a time t

R^* : effective particle radius

R_i : radius of particle i

R_p : new contact curvature due to plastic deformation

$\overline{R}$: dimensionless ratio of new contact curvature to effective particle radius

S_{12} : distance between particle centers of particle 1 and 2

v : typical speed of the material at the funnel outlet

V : volume flow rate

v : Belverloo velocity

v_t : component of velocity tangent to the contact surface

W : mass discharge rate

α : "overlap" between two particles when colliding

μ_f : coefficient of sliding frction

α_{max} : the max deformation

α_y : deformation at the pint of yield

$\dot{\alpha}$: relative normal velocity of the particles

β : damping parameter

Δs : tangential displacement during the present time-step

ρ : density of the particle flow

σ_i : yield stress

τ : characteristic time varies with particle materials and hopper openings

ACKNOWLEDGEMENTS

I would like to thank Dr. Joseph McCarthy first for his time and patiently advice both on my research and writing. I also want to thank my group members Tatha and Adel for their help. They are very knowledgeable and enthusiasm colleague. Most of all, I would like to thank my parents and my friends for all of their support and understanding over the past two years. I would also like to thank my boyfriend Tongchuan Gao, for his encouragement and assistance.

1.0 INTRODUCTION

Particulate systems play an important role in many several industries, like pharmaceuticals, polymers, mineral processing, munitions, energy, food processing, environment and agriculture [2]. However, despite extensive study, an understanding and predictive ability for the behavior of particle technology is limited.

Across particle technology, hoppers are widely used in many process engineering applications for the storage granular materials [3]. The range of hopper application is from small scale pharmaceutical, food processing operation to large scale minerals industry storage. More important than being used as storage facilities, hoppers are also often used as links between various unit operations in plant processes to provide buffering to control flow variation and operational instability. This becomes more important in a particulate solids processing plant. In this process, the bulk solids behavior is generally more unpredictable than for gases and liquids and unsteady flows often occur in the course of handling and processing and this inconsistency can lead to dramatic loss of revenue and/or delay in process start-up [2].

One of the major industrial problems in using hoppers is obtaining reproducible and consistent particle discharge flow rates. Furthermore during the particle flowing through the hopper, jamming is a common phenomenon. This issue has been investigated by many researchers over the past few years. In 2009, Junyao [4] probes a method to calculate the

properties of flow and jamming in a funnel by experiments. Based on their data and results, a comparison simulation study is made in our work.

To get a smooth and reliable mass flow rate for a specified material has long been a subject of interest to both researchers and process engineers. The hopper discharge behavior is associated with the complex flow patterns of granular materials inside the hopper and the hopper properties. In order to predict the discharge rate for the dependable design and operation of a hopper, an extensive array of empirical studies have been undertaken, such as Jenike [5], Enstad [6], Williams [7] and, more recently McGee et al. [8]. Despite the fact that these studies lead to significant insight, the large number of particles; the different hoppers and/or hopper conditions; and the instrumentation necessary to determine the parameters during the flow process can lead to a very expensive project [9]. An alternative method to study (and design) hoppers in practice is to adopt a computational approach to hopper design. The discrete element method simulation method has been widely used in the recent years in the granular flow simulation [10–12].

In the simulation of granular flows using the discrete element method (DEM) the trajectories, spins and orientations of all the particles are calculated, and their interaction with other particles and with their environment modeled. In this work, this method is quantitatively validated against a suite of experiment results obtained from collaborators.

2.0 BACKGROUND

2.1 DISCRETE ELEMENT METHOD

The Discrete Element Method (DEM) is in the family of numerical computation methods that is similar to molecular dynamic methods and is especially convenient in the simulation of millimeter-scale particle motions. Although DEM can be adapted to study many problems of engineering interest, the size of the simulation often results in a computationally intensive simulation technique, such that the application of this approach to large-scale processes is limited.

With well-developed algorithms, the computational complexity can be reduced considerably [10,11], such as to treat the discrete particles as a continuum by averaging the physical properties across the particles in a simulation cell. In contrast, DEM is well-suited to detailed study of small-scale engineering problems and it is often used to validate more large-scale-focused modeling efforts. In other words, due to its derivation from first-principal constructs, like the contact mechanics, DEM is often considered as the "gold standard" for comparison of continuum-level theories or coarse-grained models of granular material flows. Despite this prevailing usage, DEM is typically validated in only qualitative manners such as in comparison of mixing rates, or gross features of granular flows such as concentration profiles, and

a detailed quantitative validation of what parameters and modeling approaches should be used is still lacking [12].

Discrete element method simulations can be used to determine essentially any flow properties of all the particles within a granular system. It captures the macroscopic behavior of a particulate system by calculating the trajectories of each of the individual particles within the mass and the time evolution of these trajectories [13]. The particles experience forces and torques due to inter-particle interactions and interactions between the system and the particles [14]. Depending on the density and character of the flow, two different methods are available to calculate the trajectories of particles in DEM simulation. For the low density, fast flow, which is often called the grain-inertia regime, a rigid sphere model is used to describe the physics of it. Whereas for the high density, slow flow, the particle system is in the quasi-static regime [13] and a different model, the soft sphere model, can be exploited in this regime.

In general, the grain-inertia regime is controlled by binary collisions between particles. The inelasticity of the collisions is included by the collision rules through a coefficient of friction, for tangential impacts; and restitution, for normal impacts. For that reason, the flow behavior of the particles can be broken down into binary collisions and the linear and angular momentum with some collision or closure rules are kept to get the trajectories of the particles [15]. As for the idea of computation, an initial condition is preliminarily created to determine the positions and velocities of each particle before the flow ever occurs. Then the first collision time for each particle is calculated subsequently and the collisions are placed in a sequential order. The simulation process follows this order to update the changes of position and velocity for any particles involved in the current collision. Also updated is the

collision list for particles that are about to interact with the particles in the current collision. Following the path of such iteration, the trajectories of each particle can be obtained.

In terms of soft sphere model, which is the method used in the present work, the behavior of particles in this regime is characterized by lasting particle contacts. The explicit solution of Newton's equation of motion for every particle is used to calculate the particle trajectories, where contact mechanics are considered. Three types of forces build up the whole mechanical scheme of contacting particles, namely normal forces (Hertzian forces), cohesive/repulsive forces and tangential forces. From these the global flow of the granular material can be determined [16, 17].

2.2 FORCE MODELING

2.2.1 Normal Forces

For the normal forces we use two approaches in our study. They are a Hertzian spring with a viscous "dashpot" as our dissipation model [18] (which we call the "elastic model") and an elasto-plastic material model which is also called our "plastic material model" [19].

When one particle collides with another one, the shape changes and therefore the distance between the two particles will be smaller than the sum of the diameters of the two particles. For both the above two approaches, this superposition of the two particles is used in the calculation of the normal force in the simulation. The "overlap" is defined as $\alpha = (R_1 + R_2) - S_{12}$, where R_i is the particle radius and S_{12} is the distance between particle centers of particle 1 and 2. The normal force for both cases contains a Hertzian (non-linear) contribution given

by

$$F_n = k_n \alpha^{3/2} \tag{2.1}$$

where k_n is the normal force constant. This normal force constant is from the Hertz theory [20]. Also this constant is related to the particle radii, R_i, and the elastic properties. The elastic properties includes the Young's modulus E_i and Poisson ratio σ_i. k_n is calculated as follows

$$k_n = 4/3E^* \tag{2.2}$$

where R^* and E^* are given by

$$\frac{1}{E^*} = \frac{1-{\sigma_1}^2}{E_1} + \frac{1-{\sigma_2}^2}{E_2} \tag{2.3}$$

$$\frac{1}{R^*} = \frac{1}{R_1} + \frac{1}{R_2} \tag{2.4}$$

respectively.

The calculation for the normal force will be continued separately from this point for the elastic and plastic case, due to the different energy dissipation of the two models.

For the spring-dashpot model, a damping term that is proportional to the relative normal velocity between particles is used. This term is linearly added to the repulsive force form Eq. 2.1. The Oden and Martins [21] model is chosen in the study from the various forms of the new damping term since the coefficient of restitution's dependence on impact velocity, a power law decrease, more closely follows experimental results.

After adding this new damping term to the previous normal force equation, the combined equation could be written as

$$F_n = k_n \alpha^{3/2} - \beta \alpha \dot{\alpha} \tag{2.5}$$

where $\dot{\alpha}$ is the relative normal velocity of the particles, and β is a damping parameter that is used as an adjustable parameter in this work.

On the other hand, for the plastic material model, the dissipation arises from the fact that the center of a contact will exhibit plastic deformation for sufficiently strong collisions. If the normal force exceeds the material yield force, F_y, subsequent loading is given by the linear relation:

$$F_n = F_y + k_y(\alpha - \alpha_y) \tag{2.6}$$

where, k_y is the plastic stiffness, and α_y is the deformation at the point of yield. The plastic stiffness is linked to the yield force F_y, which is $k_y = (3/2)(F_y/\alpha_y)$. The deformation at the yield point shows that both Eq. 2.1 and Eq. 2.6 give $F_n = F_y$.

Unloading, using the plastic material model, follows a pure elastic model before the yield limit is exceeded. When the yield limit is exceeded, this unloading is similar to a purely elastic unloading except that the surface curvature is modified. The unloading is given by:

$$F_n = F_{max} - k_n \sqrt{\overline{R}} (\alpha_{max} - \alpha)^{3/2} \tag{2.7}$$

where F_{max} is the maximum force, α_{max} is the deformation, and $\overline{R}$ is given by the ratio of R_p to R^*, where R_p is the new contact curvature due to plastic deformation and R^* is still

the sum of the reciprocal of the two particles' radii. The $\overline{R}$ is dimensionless and it can be written as

$$\overline{R} = \frac{R_p}{R^*} = \frac{F_y}{F_{max}}(\frac{2F_{max} + F_y}{3F_y})^{3/2} \tag{2.8}$$

The particles' normal force would start from Eq. 2.7 again when another loading is needed after the initial yield. Because there is a prior force and the contact continues to deform plastically as Eq. 2.6.

Similarly to the damping parameter discussed in the previous paragraphs, β, the yield force, F_y, is loosely related to the yield stress of the bulk material and, in this work, is treated as an adjustable parameter.

2.2.2 Tangential Forces

In contrast to the procedure for calculating the normal force between the particles, the variety of methods for modeling the tangential forces cover a considerably wider range of approaches. When choosing a tangential forces model, we first eliminate any models which obtain the tangential force directly from the tangential velocity for the reason that these types of model will lead to particle creep (an aphysical result). The simplest of the "history dependent" friction models is used in our study as the tangential force model [13], while we plan to incorporate the most comprehensive model [22] for later tests (as needed). The tangential force, F_t acting at a particle-particle contact for each time-step in this history-dependent friction model is given by

$$F_t = F_{t0} - k_t \Delta s \tag{2.9}$$

where, F_{t0} is the old tangential force, k_t is the tangential stiffness, Δs is the tangential displacement during the present time-step, and $k_t \Delta s$ is the incremental change in the tangential force during the present time-step due to the relative particle motion. The tangential displacement Δs could be interpreted as $\Delta s = v_t d_t$, where v_t is the component of velocity tangent to the contact surface and d_t is the time step.

The tangential stiffness, k_t, in the above equation can be assumed as a constant in the currently employed friction model, and this constant is written as k_{t0}. Comparing this tangential stiffness k_{t0} to the normal stiffness k_n [20], their ratio is

$$\frac{k_n}{k_t} = \frac{ds/dF_t}{d\alpha/dF_n} = \frac{1-\sigma/2}{1-\sigma} \tag{2.10}$$

where all the parameters have been given in the previous paragraphs. This relation assumes that the rates of change of displacement with loading should be similar for tangential versus normal interaction. Finally, we incorporate a discontinuity in order to limit the tangential force to the Amonton's Law limit such that $F_t \leq \mu_f F_n$, where μ_f is the coefficient of sliding friction.

3.0 GRANULAR FLOW

3.1 BEVERLOO'S EQUATION

The hopper discharge rate, as a dependent variable of both the nature of particles and hoppers, has been related to many parameters through the past many years. Research in early years proposed that the mass discharge rate W should be dimensionally proportional to $\rho g^{1/2} D^{5/2}$ [23], where ρ is the density of the particle flow, g is the acceleration due to gravity, and D is the hopper opening size. This expression can be motivated in a straightforward way, provided that the fill height is assumed to not affect the discharge rate (that is, the pressure in a granular column is not hydrostatic in nature). During the outflow process, the mass flux is given by $j = \rho v$, where v is the typical speed of the material at the funnel outlet, and ρ is the mass density of the flow. The mass flow rate, then, is calculated as $W = jA$, where A is the hopper outlet area.

In a hopper with an outlet of circular cross-section, the area is given as $A = \pi(D/2)^2$, which is about the same magnitude as D^2. In this case,

$$W = jA = jD^2 = \rho v D^2. \tag{3.1}$$

If one imagines that material fluidizes up to a height D, we can take the characteristic length of the flow to be D. Therefore, the exit speed can be approximately considered to be the speed of a falling particle starting with zero velocity after distance D with the accelerate g. It is shown as follows:

$$v \simeq (gD)^{1/2}. \tag{3.2}$$

However, this approximate model is restricted, because the walls will exert a drag force. Hence, there exists a boundary layer effect, which reduces the opening diameter D to an effective value depending on the particle size. This above mass flow rate equation cannot match with the results of several experimentalists. Along with many experiments have been made, it is pointed out that the discharge rate varies slightly more with the outlet width than what it is shown in the preceding equation. Rather than 2.5, Franklin and Johanson [24] got the result with a power of 2.93, and Brown and Richards yielded it as 3.1 [25]. Finally, in 1961, Beverloo *et al*. gave a comprehensive explanation of the flow behavior and also a supplement on this equation to the previous findings [26].

In the study of Beverloo, a variety of materials were used and the results were compared. The materials used included sand, linseed, spinach, watercress, rapeseed, kale, swede, and turnip. These materials represented particles with different properties, such as density, spherical diameter and so on. These particles were set to flow in four different kinds of orifices: circular orifices, square orifices, rectangular orifices, and triangular ones. Furthermore, seven different opening diameters, ranging from 0.22 cm to 4.02 cm, were designed for each apparatus. They concluded that the particle size influenced the particle flow. This influence decreased along with the increasing of the ratio D/d, where D is the diameter of the orifice

and d is the size of the particles. The plots about $W^{2/5}$ versus D have been made based on the results. It showed a linear relationship, and the intercept on the abscissa is taken as a value Z. This Z is related to the effective grain particle diameter d_e and the material dependent constant k, which can be interpreted as $Z = kd_e$. Due to the effect of the area around the hopper outlet on the particles, this intercept Z is for adjusting the outlet value. Therefore, the Beverloo equation for 3D hoppers has been put forward as [26]:

$$W_{flat\ bottom} = C\rho g^{1/2}(D - kd_e)^{5/2} \tag{3.3}$$

where ρ is the bulk density of the material after filling the hopper, g is still the gravitational acceleration, k is the Beverloo constant depending on the particle geometry, C is an empirical constant which ranges from 0.55 to 0.65, $W_{flat\ bottom}$, d_e, and D, as have been mentioned before, are the mass flow rate, the mean particle diameter, and outlet opening size respectively. This equation can also be linked to the volume flow rate V as:

$$V = Cg^{1/2}(D - kd_e)^{5/2} \tag{3.4}$$

If the width of the hopper is narrow enough between the front side and the backside that only a single layer of the particles can be flowing in the hopper, we can then consider this kind of hopper as a 2D hopper. After some brief modification on the original 3D Beverloo equation, the hopper opening varies as the first power of D, and the 2D Beverloo equation becomes:

$$V = Cg^{1/2}(D - kd_e)^{3/2} \tag{3.5}$$

3.2 HOPPER DISCHARGE RATE

In addition to the effect of the hopper outlet, various other parameters impact the discharge rate from a hopper as shown in the Beverloo equation mentioned above. This issue has been investigated by lots of studies [27–30]. Also in the study of Anshu *et al.* [1], a full-scale investigation was made to find out the parameters affecting the discharge rate using the discrete element method. A review of these efforts is outlined below.

3.2.1 Fill Height and Friction

The discharge rate is usually assumed to be unrelated to the initial fill height of the hopper. In Anshu's work, four parallel tests have been made: the base-case fill-height, double fill-height, triple fill-height, and quadruple fill-height. First, a small friction coefficient which is 0.05 is used as shown. With this small friction coefficient, the mass flow rate grows from 163.9 g/cm/s for the base-case fill-height to 220.1g/cm/s for the quadruple one. The friction coefficient 0.84 was then taken in the simulations with the previous four different fill-heights. With this larger friction coefficient there is almost no difference observed for the mass flow rates of these four different initial fill height. The base-case fill-height got a mass flow rate of 111.0 g/cm/s, and for the quadruple one the mass flow rate is 109.0 g/cm/s. In the plot of time versus mass flow rate drawn in their work, all lines became the same slope for this bigger friction coefficient [1]. With this result, the assumption that the discharge of coarse granular materials is generally independent of the fill height can be supported.

Additionally, there are another 6 sets of studies with the friction coefficient 0.005, 0.1, 0.15, 0.2 0.5 and 0.84 for these four different initial fill height. These six sets of studies

illustrate how the fill height versus discharge rate varied with the change of the friction coefficient. For the first three friction coefficient values (0.005, 0.1 and 0.15), the discharge rate is obviously increases when the fill-height is increased; however, the slopes in the discharge rate versus fill-height figures became more gradual as the friction coefficient becomes bigger. When the friction coefficient is 0.2, it can be seen that a horizontal line is obtained at a certain discharge rate value, which means that the discharge rate did not change with the fill-height anymore. It can be inferred that the discharge rate is not dependent on the fill-height when the friction coefficient is 0.5 or 0.84 either [1].

It could be concluded that this influence from the initial fill height can be ignored when the friction coefficient is bigger than 0.2. In practical experiments, the friction coefficient generally should be at least 0.2 or more according to published experimental studies [30]. Thus, the discharge rate from the hopper is not related to the initial particle fill height.

3.2.2 Particle-particle and Particle-wall Friction

There are two kinds of friction in the hopper discharge process: particle-particle friction and particle-wall friction. In general, the particle-particle friction has a larger effect on the hopper discharge than the particle-wall friction.

In the same study of Anshu, several comparisons were made between the effects of the discharge rate by these two friction types. In the base case friction condition, the friction between particle and particle is 0.2, while that between particle and wall is also 0.2. In the large particle-particle friction case, the particle-wall friction is still 0.2 while the particle-particle fraction increased to 0.84. In the large particle-wall friction one, the particle-particle friction is 0.2 and the particle-wall friction is 0.84. The large particle and wall friction trial

considers both the particle-particle and the particle-wall friction to be 0.84. Among these four sets of trials, the results show that they can be considered as two pairs. The base case friction one is similar to the large particle-wall friction one, since their instantaneous discharge rates are almost the same as time goes by and their final discharge rates are both 140.4 g/cm/s. The other two trials also have similar results, yielding discharge rates of 114.7 g/cm/s and 114.1 g/cm/s [1], respectively. This could be generalized that the discharge rate is primarily related to the particle-particle friction, and the particle-wall friction has little effect on the discharge rate.

Jiyu *et al*. built a model to predict the flow rate of granular system from a hopper [31]. It was shown that the shear friction between the particles needs to be taken into account. Their research also proved that Beverloo's equation was most recommended to predict the solid flow rate of an orifice discharge.

3.2.3 Hopper Width

In the study of Nedderman *et al*. [3], the hopper width was proved to have little impact on the hopper discharge rate, if the hopper is with large hopper outlet and is discharged only by gravity. Due to Janssen effect, when the granular layer is more than 1.2 times larger than the diameter of the hopper width, the flow rate is a constant in the hopper discharge process. It was shown that if the diameter of the hopper width is 2.5 times greater than the diameter of the hopper outlet and, at the same time, also greater than the sum of hopper outlet diameter and 30 times of particle diameter, the hopper discharge rate will be independent of the hopper width.

Referring once again to the study of Anshu [1], a comparison by DEM simulation has been made between the discharge rate of two hopper widths. One is the base case and the other one has hopper width twice as big as the base case. In order to keep the same initial particle fill height, the double hopper width case has twice the amount of particles as the base case hopper width. Therefore, the double hopper width one took twice the time to empty as the base case. This also demonstrates that the hopper width does not influence the granular flow rate.

3.2.4 Hopper Angle

The hopper angle plays a very significant role in the hopper discharge rate, second only to the influence by the hopper outlet width which will be talked about later. In general, the discharge rate decreases with an increase in the hopper angle.

The following figure 1 descriptor the discharge rate which is regard to the hopper angle with the data from Anshus DEM simulation, Brown and Richards's results [32,33] and Rose and Tanakas [34]. In Brown's study, a set of experiments were carried for different angles, with 0.32 cm as the diameter of the ball bearings and also with a single layer flowing in the hopper. Although there are some differences among the curves on the plot, the trends for these lines are all the same. From hopper angle around 20° to 55°, the discharge rate goes down. In the slowly descended curve, 55° is a turning point. For the DEM simulation case, the discharge rate declined much more slowly than the angles before 55°. The discharge rate seemed to be not change when the hopper angle is bigger than 55° in the Rose and Tanaka's empirical results. While the Brown and Richards shows that the flow rate slightly goes up when the hopper angle increase from 55° to 90°.

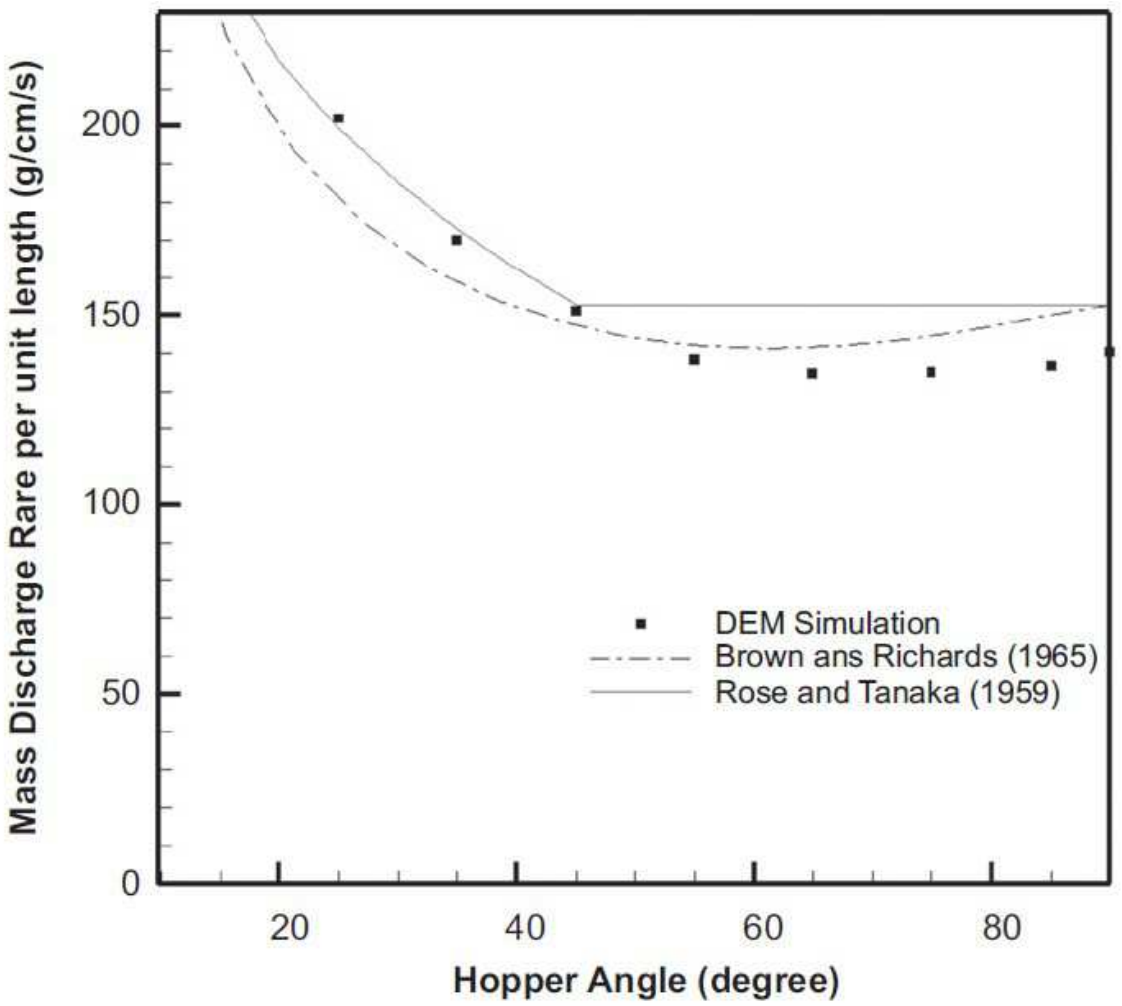

Figure 1: DEM mass discharge rate plotted against hopper angle [1]. The correlations by Brown and Richards and Tanaka are also plotted.

3.2.5 Outlet Width

The hopper outlet is the most important parameter impacting the hopper discharge rate, as it were. It has been clearly written in the Beverloo equation as given a reference in the previous paragraphs. A lot of research has been devoted to the hopper discharge rate and the Beverloo equation, since this is the most widely accepted law that can predict the flow rate of the granular flow from a hopper. As is clear from the Beverloo equation, $V = Cg^{1/2}(D - kd_e)^{3/2}$, the discharge rate increases exponentially with increasing hopper opening.

4.0 PROBABILISTIC MODEL

In this work, we compare our simulation results to a series of experiments carried out by Duke University. A schematic of the apparatus is sketched in the figure 2 below [4]. The hopper is built up as a pseudo-2D one. Plexiglas plates, which are spaced slightly more than the thickness of the particles, are used as the front and backsides of the hopper. The plates all are composed of approximately 0.32 cm thick PSM sheets, which are manufactured by Vishay Inc. Hence, these two plates determine the flat shape of the hopper. Two pairs of triangular aluminum spacers form the internal walls of the hopper. The spacers have tilted sidewalls and can be shifted laterally to change the opening size of the outlet. The two sets of spacers are placed symmetrically about the hopper opening. In addition, a pair of slats, which can be pulled outwards in order to initiate flow, closes the hopper opening when the system is idle. With the hopper design, one can repeat the flowing process effortlessly by simply flipping the hopper.

The particles in their experiments are disk-like ones with two diameters. One is 0.770 cm, accounting for 38% of the total, and the other is 0.602 cm, which accounts for 62% the number of the particles. This binary mixture is used in order to minimize the impact of crystalline packing formation (a phenomena that is particularly prevalent in 2D particle beds). There are approximately 8750 such disks inside the hopper. The nominal elastic

modulus of the particles is 4.8 MPa, and the static friction coefficient is measured to be between 0.7 and 0.8. The width of the hopper is 43 cm and the height between the top opening and the outlet is approximately 100 cm [4].

In the initial stages of an experiment, all of the particles are above the opening and the hopper is vertical displayed. A slide plate is on the hopper outlet which is moved in order to initiate flow of particles to the lower half of the apparatus. After all the particles have left the upper half of the apparatus, which means all the particles passed through the hopper outlet, the time since the start of particle flow is considered to be the empty time for this given angle and hopper opening size. The hopper angle is the angle between the hopper wall and the horizontal line at the opening. Once one experiment is done, the apparatus will be flipped vertically so that another experiment can start immediately. The experimental apparatus can have different hopper angles including 0, 15°, 30°, 45°, and 60°. At the same time, the hopper opening size can take values of 2.9 cm, 3.1 cm, 3.3 cm, 3.5 cm, 3.7 cm, 3.9 cm, 4.1 cm, 4.3 cm, and 4.5 cm for each angle.

In Duke's study, a new, probabilistic approach to jamming in hopper flow was proposed, which is suitable for simple non-cohesive particles. The key point of this approach is that: the particle falling speed at the hopper opening is dependent on the opening diameter, instead of the particle height, which is substantiated by the assumptions that the Beverloo equation is valid [35–37]. As an experiment proceeds, it is common for the the flow to be interrupted due to the occurrence of jamming. In order to develop a probabilistic mathematical model, several simplifying assumptions are made. First, the flow rate is assumed to be constant. Then, the probability that a jam occurs in a very short time interval, dp_j, is expected to depend only on the length of this interval, dt, and is assumed to be independent of the

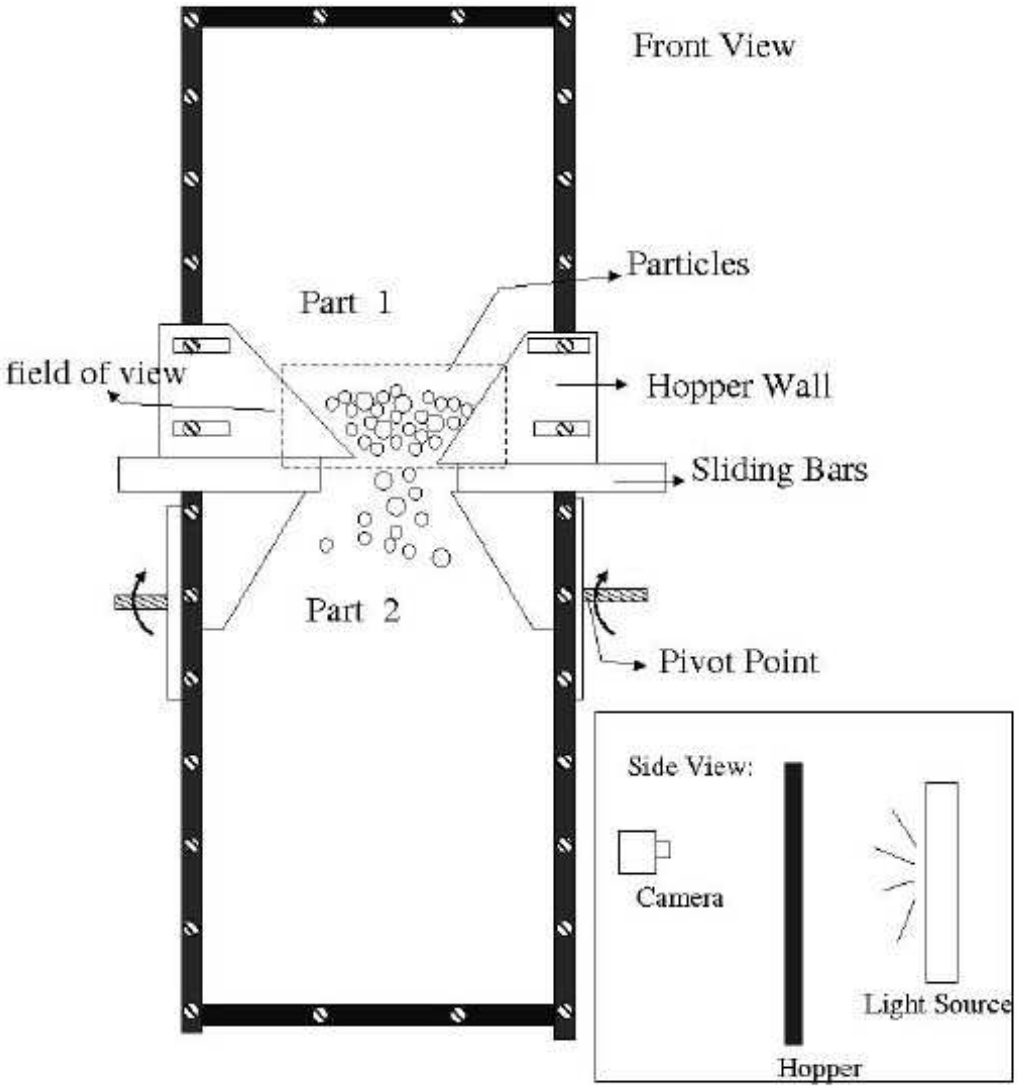

Figure 2: The schematic of hopper (used by permission)

particle configuration or the time elapsed since flow initialization. The primary probabilistic relationship can then be written as $dp_j = dt/\tau$, where τ is a characteristic time that varies with particle material properties and hopper openings. This model, therefore, depends exclusively on a phenomenological time, τ.

To develop the consequences of this model further, they consider the probability that a flow has survived for a time t without suffering a jam, $P_s(t)$. If $P_s(t)$ is known, then $P_s(t + dt) = P_s(t)(1 - dt/\tau)$, which then gives

$$P_s(t) = \exp(-\mathrm{t}/\tau) \tag{4.1}$$

since $P_s(0) = 1$ (and assuming that the coefficient τ is a constant).

With this probabilistic equation and the Beverloo equation that was mentioned previously, one can predict the probability of jamming for a given fill volume. The fill volume is related to the hopper initial condition, with a mass M or a volume V. As the flow rate is assumed to be constant, which on average is a very good approximation, the survival equation could be reformed as

$$P_s(V) = \exp(-\mathrm{V}/(\dot{\mathrm{V}}\tau)) \tag{4.2}$$

Based on this developed equation, if there are two initial fill volumes V_1 and V_2 for a fixed material type, the survival probabilities for the two different fills could be obtained as

$$P_2(V_2) = (P_s(V_1))^{V_2/V_1} \tag{4.3}$$

This equation shows the probabilities that all the particles are completely discharged from the hopper and no jam happens.

If the probability that a jam happens is taken to be p_j and, on the other hand, the probability that the system flows without a jam is p_u, then $p_u = 1 - p_j$. Under the condition that the particle diameter is d and the jamming is mainly determined by the particles flowing near the outlet, a time range τ_g can be defined as $\tau_g = d/v$, where v is the Beverloo velocity. If we further assume that the initial effects are not important, then during a short time dt, we use $dt = \tau_g$ to get the probability that a jam happens. Therefore, we have $p_j = dt/\tau = \tau_g/\tau$. So that,

$$\tau = \tau_g/p_j \tag{4.4}$$

When particle properties, the opening angle and hopper wall properties are given, p_j can be uniquely dependent on the ratio d/D. When d/D approximately equals to unity, we have $p_j = 1$. While as d/D approaches to zero, we have $p_j = 0$. Another assumption can be put forward on dimensional grounds, that

$$\tau = \tau_g/p_j \ \simeq \ (d/g)^{1/2}[(D - kd)/d]^{\alpha}. \tag{4.5}$$

In the experiments, a measurement of the time between the beginning of flow until a jam occurs is used to calculate the probability distribution of the jamming time. The measurement was repeated 100 times and the survival time was calculated based on the exponential decay probability density function.

To further elucidate their assumption, a high-speed video (with polarizers) was taken. Since the polymeric beads used in the experiment are birefringent, the polarizers allow one to visualize stress levels within individual particles. Therefore, the video shows the pressure profile of the particles and we use this (as well) in comparison with our simulation. Video

without the polarizers is also taken in order to track the particle positions and obtain a particle velocity profile, which is also compared to our simulation results.

5.0 SIMULATION RESULTS

5.1 SIMULATION SETUP

In the simulation, we set the particle diameter to be a mixture of 0.77 cm and 0.602 cm beads (as in the experiment). The former and the latter disks account for 38% and 62% of the total number [4], respectively, in both cases (simulation and experiment). Moreover, the total number of simulated particles is 8750, which is exactly the same as the number used in the experiments. Spherical particles are used in the simulation, rather than disks (as in the experiment) because it is assumed that a small aspect ratio cylinder will behave very similarly to a sphere. In our simulations we treat the static friction coefficient is treated as an adjustable parameter, where we use the empty time of angle 15° and opening size 4.5 cm from the experiment result has been used as the baseline for our study. To best match our simulation results to the experiment results, we find that the static friction should be 0.5 rather than 0.7 - 0.8, which was quoted in the experiments. Our initial attempts in model comparison used the plastic model with no slide damping, as this was the most successful model in our previous validation efforts [12].

5.2 EMPTY TIME FOR HOPPER DISCHARGE

In the experiments, researchers can actually see the particles going through the opening of the hopper and photographs are taken from a camera with a certain frequency. The empty time is then obtained via direct inspection of the photographs. When it comes to the simulation, one can also depict the configurations of the particles in the undergoing emptying process frame by frame, just like what experimentalists do with a camera, based on files we obtained through simulation; however, we took a simpler and sometimes more accurate method than reading and counting the photographs to get the empty time. In this study, the position of the top-most particle inside the hopper is monitored to get the empty time. According to this method, the moment the highest particle is below the hopper opening is considered to be the empty time.

Figure 3 shows the configuration of the flowing particles in the hopper, whose hopper angle is 15° and opening size is 4.5 cm.

This frame of the picture is picked out at a randomly selected moment. This picture shows roughly the 300th frame captured by the simulation, which illustrates the particle configuration of the 10th second since the flowing starts, because we set the frame per second to be 30, which means 30 files are generated per second in the simulation.

One can clearly discern the location of the hopper walls from this figure by direct inspection. The hopper walls are built mathematically so that there is a smooth barrier at the right and left edges and then a (user-defined) hopper angle between hopper walls and the horizontal plate, and finally a gap in the wall representing the hopper outlet. Thus the wall slope is the tangential value of the hopper angle. In order to calculate collisions between

Figure 3: The configuration of the flowing particles in thie hopper for angle 15° and opening size 4.5 cm by DEM simulation.

the particle and wall, we start with a particle whose x position is x_0. The equations for the hopper walls on the coordinate axis can be written out in response to the different angles of the hopper. The distance between the particle and the wall can be calculated with the known coordinate of the particle as (x_0, y_0). Then the position of the wall could be obtained. Take the left slope hopper as an example, if the distance between one particle and the wall is d_1, than we use $x_0 - (d_1 \sin(\textit{hopper angle}))$ to describe the hopper wall. The right slope wall could be calculated in the same way.

During the particle flowing experiment, jamming occurs probabilistically. When jamming occurs, all the particles get stuck and stay still. The system cannot resume the motion spontaneously. Therefore, in much the same way as in the experiments, an external force must be introduced to the hopper. For example, a single pendulum is often used to regain the flow in the hopper in experiment and industry. To mimic this jam-removing method in simulation, small velocities are assigned to all the jammed particles. The velocities are minor enough that the positions of all the particles are not to vary in a short time interval. The velocity being added to each particle is called "kicking velocity".

The following figures (figure 4-8) show the comparison of experimental and computational results for the hopper empty time. As the legend suggests, the open diamonds represent the computational data for the plastic particles, the open circles are for the elastic particles, and the solid circles represent the experimental data from the study carried out at Duke University [4].

Since the static friction coefficient is determined in the computational scripts based on the experimental empty time of angle 15° with the opening size 4.5 with plastic materials, figure 3 naturally shows the best fit between the computational data and the experimental

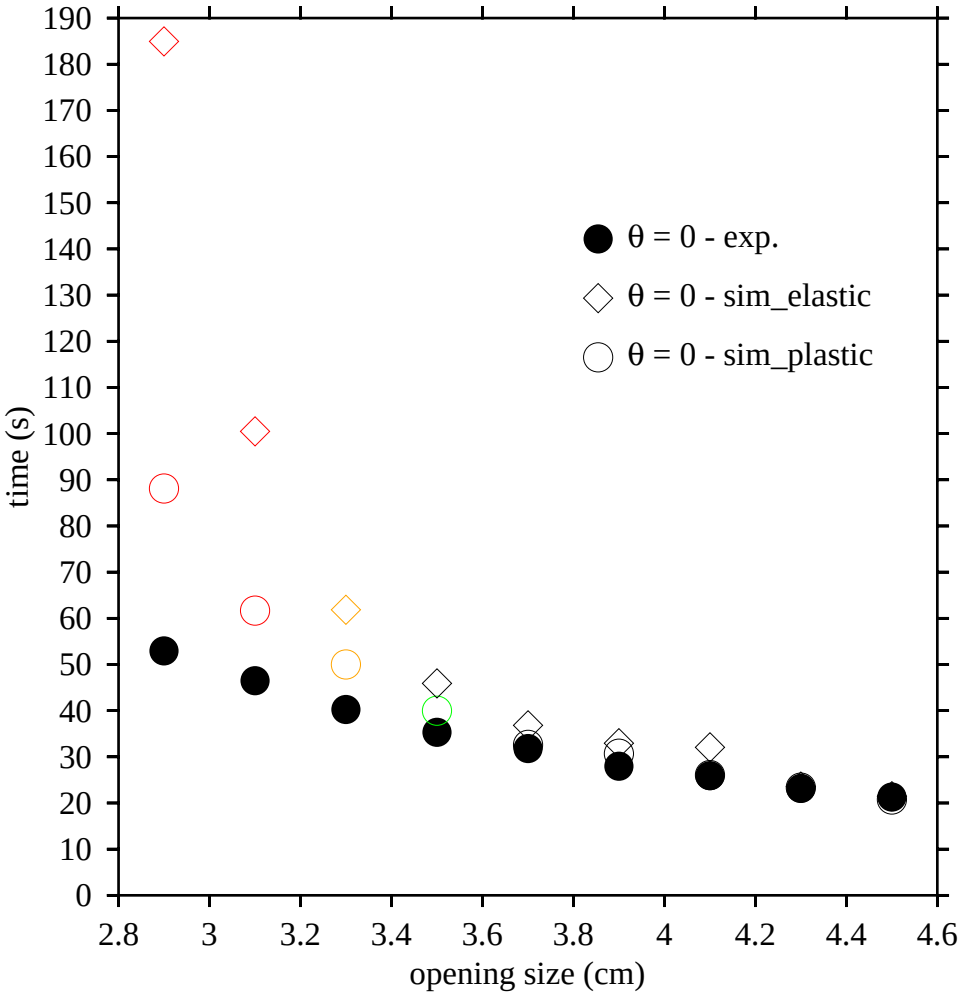

Figure 4: Comparison of experiment (solid bullets) and computational results of both elastic material (open diamond) and plastic material (open circle) for the 0 degree hopper's empty time. The different colors stand for different numbers of times of jams during the discharge process for both the elastic and the plastic materials of the computational data.

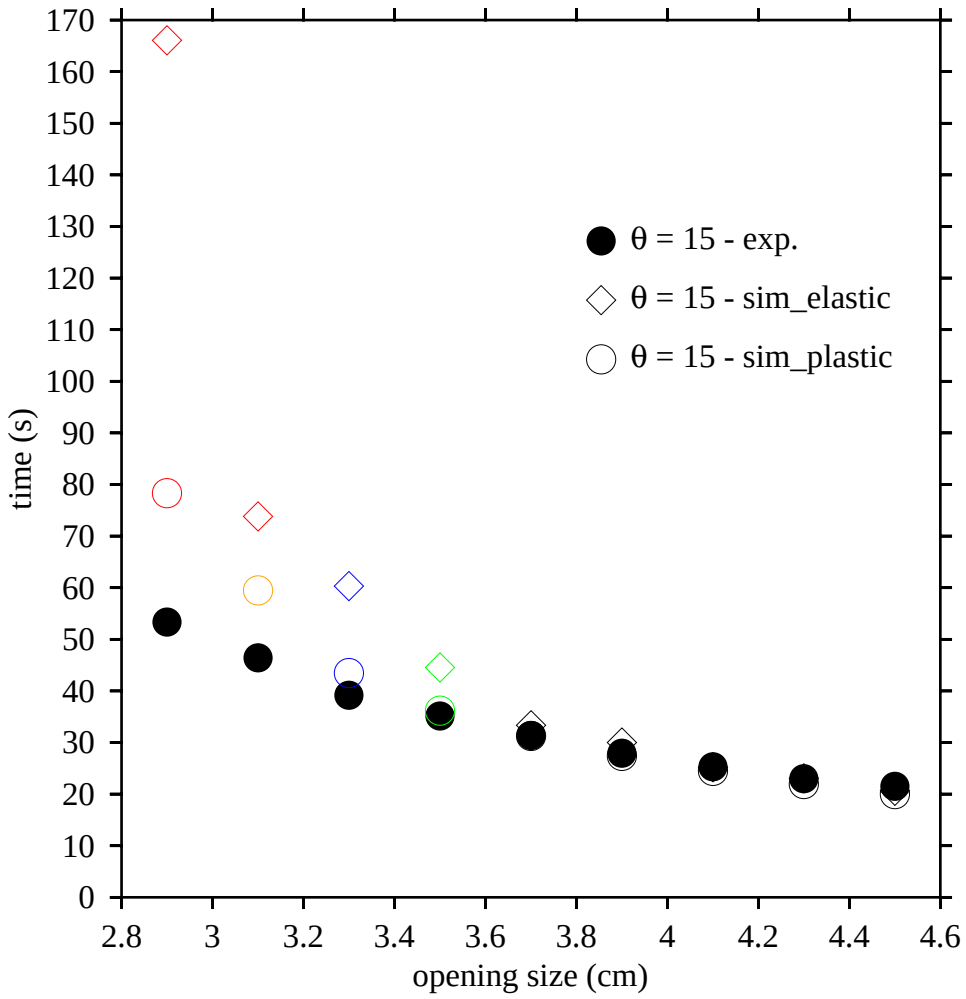

Figure 5: Comparison of experiment (solid bullets) and computational results of both elastic material (open diamond) and plastic material (open circle) for the 15° hopper's empty time. The different colors stand for different numbers of times of jams during the discharge process for both the elastic and the plastic materials of the computational data.

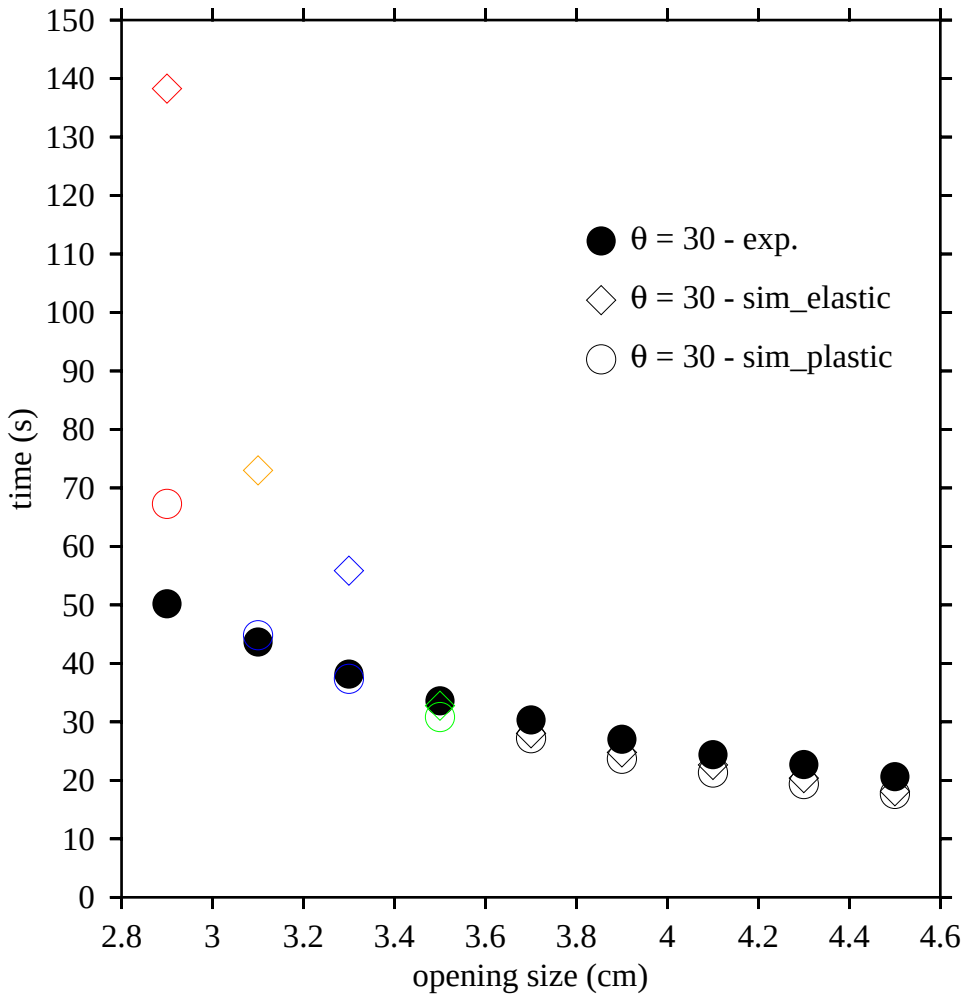

Figure 6: Comparison of experiment (solid bullets) and computational results of both elastic material (open diamond) and plastic material (open circle) for the 30° hopper's empty time. The different colors stand for different numbers of times of jams during the discharge process for both the elastic and the plastic materials of the computational data.

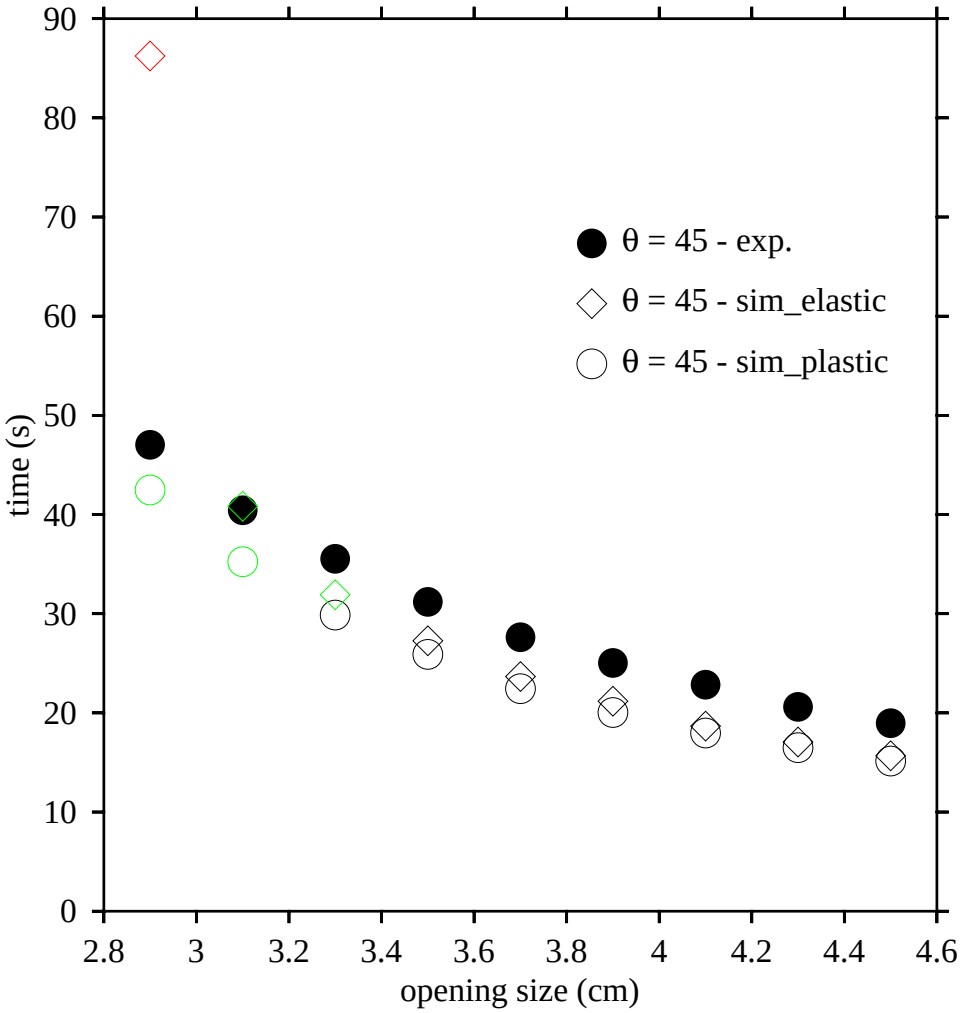

Figure 7: Comparison of experiment (solid bullets) and computational results of both elastic material (open diamond) and plastic material (open circle) for the 45° hopper's empty time. The different colors stand for different numbers of times of jams during the discharge process for both the elastic and the plastic materials of the computational data.

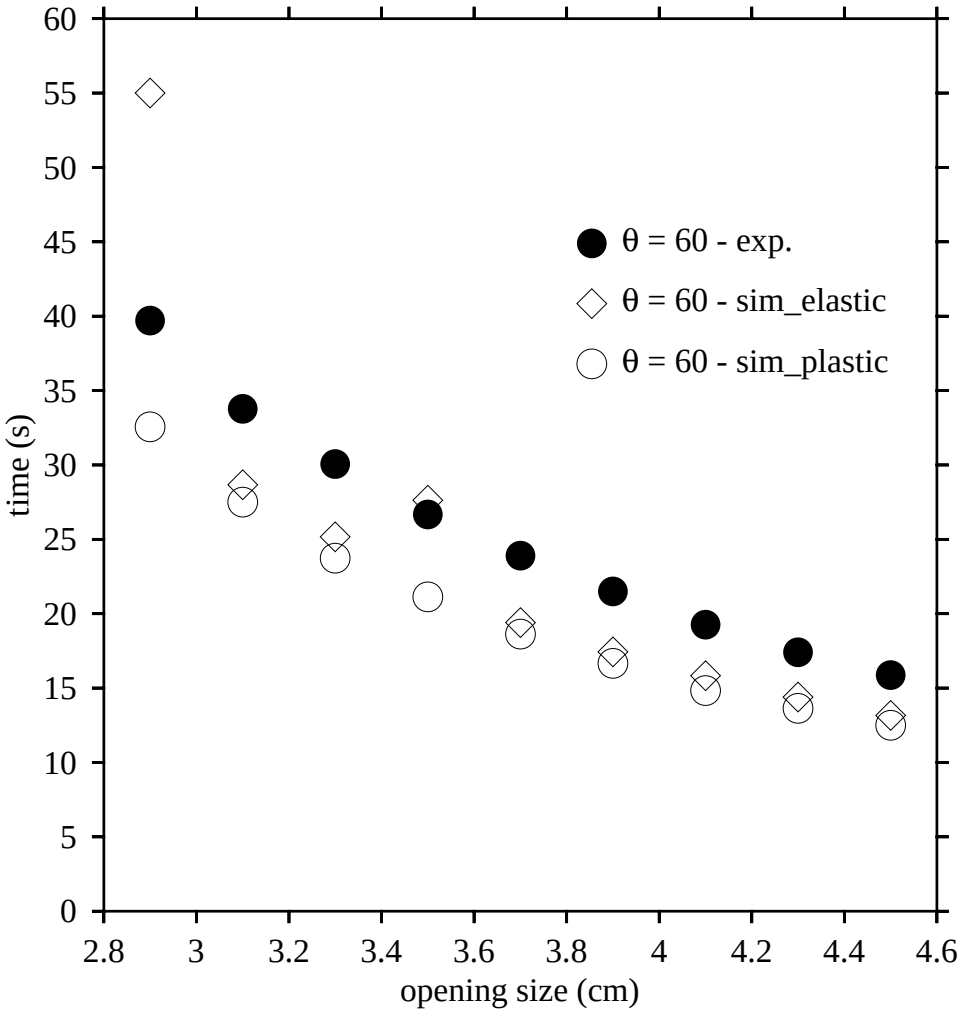

Figure 8: Comparison of experiment (solid bullets) and computational results of both elastic material (open diamond) and plastic material (open circle) for the 60° hopper's empty time. For 60 ° hoppers with different opening size, all the bullets are black, which stands for that no more than 5 times of jams happened in the simulation for both elastic and plastic materials.

data among conditions of all hopper angles. Another observation is that, of all the five figures, the larger opening sizes display better fitting between the three data points for any given angles.

In the plots, five different colors are used to show how many jams that occurred in the hopper discharge process. Red marking indicates that there are more than 50 times of jams happened from the beginning to the hopper empty. Like wise, orange is for 35 to 49 times, blue is for 15 to 34 times, green is for 5 to 14 times, and black is for 4 times of jams or less. According to these five plots, in general the more jams during the discharge process the more deviation between the computational results and the experimental results.

We should point out that the angle 0 degree should be considered a special case, where the hopper has a "flat" bottom. The particles near the sidewalls of the hopper actually cannot flow toward the opening along the bottom, as is the case for non-zero angled hoppers (figure 9). As a result, some particles can never entirely vacate the hopper with angle 0. Hence, the method of empty-time calculation previously mentioned, namely the upmost particle monitoring method, is not applicable in this case. As an alternative, schematic pictures are generated according to each simulation and movies are made afterwards based upon these pictures. The movie is played and the time at which the particle flow through the hopper opening becomes unchanged with time is identified by inspection. In this way, we obtain a similar empty time to that obtained in experiments from observation for 4.5 cm opening, which is closest in geometry to the baseline situation.

All of the three sets of data points in all of the figures present certain exponential trends. According the Beverloo equation for a 2D hopper, the exponential form of the flow rate $V^{2/3}$ is proportional to the opening size. Therefore the empty time vs. opening size plot could be

shown to have an exponential shape as the Beverloo equation describes. As figure 9 shows, for hopper with angle 0 degree, the empty time obtained through simulation for particles made from both the elastic materials and the plastic materials are generally higher than the ones obtained from experiments. The data fitting is improved for the bigger opening, namely from 3.7 cm to 4.5 cm opening, when compared to the smaller ones. While for the smaller opening sizes, taking the opening size of 2.9 cm as an example, large differences in empty time lay between the simulation and the experiment, regardless of the elasticity or plasticity of the particle materials. It will take only 53 seconds to empty the hopper in practical experiments, whereas the empty times in the simulations are as long as 88.1 seconds and 184.967 seconds for the plastic and elastic materials, respectively.

Furthermore, the difference in empty time between the experiments and the simulations could affect the occurrence of jamming at the hopper opening. The smaller the opening size and the hopper angle, the more likely it is that jamming will take place during the particle flowing process. The jamming frequencies in our simulations are basically much higher than those in the experiments, due to the much longer empty time. For the jamming scenarios, details will be presented in the following several paragraphs and the probability plots will be introduced.

As was stated in the forgoing paragraphs, angle 15° and opening size 4.5 cm is used as the standard for all the other sets of simulations. Consequently, 15° hoppers with any opening sizes also give the best match between theory and experiment among all angle hoppers, as shown in figure 5. As in the case of the 0 angle hoppers, for this hopper angle the smaller the opening size is, the better the fit is. Also likewise, the plastic materials still show better fit than the elastic ones. From figure 6 to figure 7, we can observe that the simulation

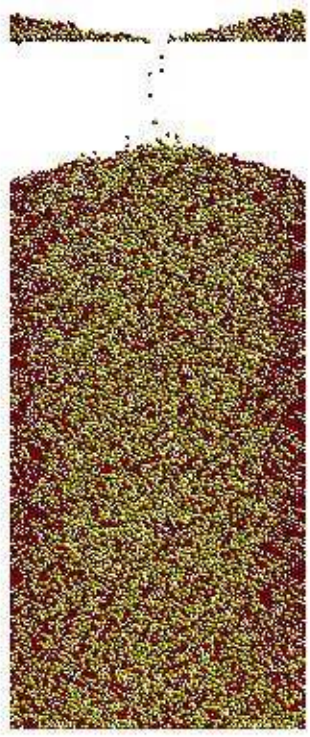

Figure 9: The configuration of the flowing particles in thie hopper for 0 degree angle by DEM simulation when the hopper is nearly empty.

data deviates from the experimental data more and more as the degree of the hopper angle increases. The empty times obtained from the simulation are all smaller than the ones in the experiment for the opening size ranging from 3.5 cm to 4.5 cm, except for the plastic model in hopper angle 60° with opening size 3.5, which seems to be a singularity in the simulation. When the angle comes to 60°, as shown in Figure 6, the deviation between simulation and experiment becomes unusually large. Even the biggest opening size 4.5 cm, the difference between simulation and the experiment is still obvious. For hopper angle 60°, the empty times from simulations are 12.5 seconds for the plastic materials and 13.17 seconds for the elastic materials, while it is 15.87 seconds in the experiment.

As mentioned before in the background part, the hopper angles play a significant role in the particle flow rate, and subsequently in the empty time of the particles. The empty time decreases as the hopper angle increases in both the experimental data and the computational counterpart. As can be seen from this set of figures, from hopper angle 0 degree to hopper angle 60°, the differences between the simulation and the experiments becomes larger.

In general, the empty time obtained through both the simulations and from the experiments decreases when the hopper angle increases; however, the decreasing rate of empty time for simulation is higher than which for experiments. When the hopper angle is 0 degree and the hopper opening is not too small, the computational empty time is slightly longer than its experimental counterpart. When the hopper angle increases up to 15°, the empty time for both are generally the same. When the hopper angle is more than or equal to 30°, the empty time obtained in the simulation is smaller than the experimental result.

In general, the observed trends of empty time evolution for both the simulations and the experiments are in good accordance with published research. In the simulation, the

geometry of the particles is spherical while, in contrast, cylindrical particles are used in the experiments mentioned. Intuitively, the empty time for spherical particles will be shorter than that of other shapes. Moreover, while we have used a binary size distribution in both the simulations and the experiments, the simulations utilized an idealized bimodal distribution (i.e., identically two sizes only), while the experiments likely have some (non-defined) particle size distribution for each mode. Again, intuition would suggest that particles with a wider spread of sizes will take a longer time to empty than that with idealized distributions, and we would expect that jamming would be more likely for multi-sized particles. Therefore, it is not unexpected that there is qualitative, but not completely quantitative agreement between the numerical study and the experiments.

To compare the data obtained from the experiments and the simulations in depth and see how well they match the Beverloo equation, we plot a function of the mass flux against opening size. The total particle mass given by Duke's study is 1024.65 g. This mass has also been used to calculate the flux value from the computational data. The flux is calculated according to the following formula $Flux = Total\ mass/Empty\ time$.

According to the Beverloo equation, for a 2D hopper, we have the relationship $V = Cg^{1/2}(D - kd_e)^{3/2}$. If we choose to plot opening size on the x-axis and flow rate to the 2/3 powers as y-axis, we expect the plot to present a linear relationship. Also, for one particular hopper opening size and the same particle materials, using identical experimental or computational methods, all the fitting lines for every angle should have the same intercept on the x-axis, since C and k are material-dependent constants, g is the acceleration due to gravity, and d_e is an effective grain diameter which may be taken, as in the studies by Mort and Geiger (cite needed) to be $d_e = d_{30}$.

As figure 10 shows, the experimentally measure flux to the order of 2/3 against the opening size does yield all the fitted lines with a y intercept of 0.95 and the slope varies from 3.7238 to 4.4918 as the hopper angle varies from 15° to 60°. This figure agrees with the Beverloo equation very well.

Figure 11 is a similar plot for the plastic particle simulation. All of the lines have a common y intercept, which is read from the plot to be 1.50923. The slopes of theses lines range from 5.076 to 5.5762 as the hopper angles increases from 0 to 60°. The difference from these constants between the simulation and the experiment could also be explained by our previous logic, that is, that the shape of the particles and the mixture of different particles do not have the same physics.

Figure 12 shows a plot of the flux versus opening size plot, but for the elastic materials from the simulations. The fitting lines for the elastic ones have an intercept of 2.0162, which is clearly larger than the intercept obtained in the plastic case. The slopes of the elastic materials from hopper angle 0 to 60° are from 5.5322 to 7.2161, which are also larger than the plastic materials and the experimental ones for each corresponding angle.

5.3 SURVIVAL TIME

In addition to examining the empty time for each realization of the hopper, we have also examined the probabilistic behavior of the jamming phenomena in this particle flow. To start with, twenty multiple simulations, in which different initial conditions were used, have been done using a plastic material model and hopper angle 30° with opening size 3.5 cm. In this case, a number of jams are exhibited (often in one simulation run). As mentioned in

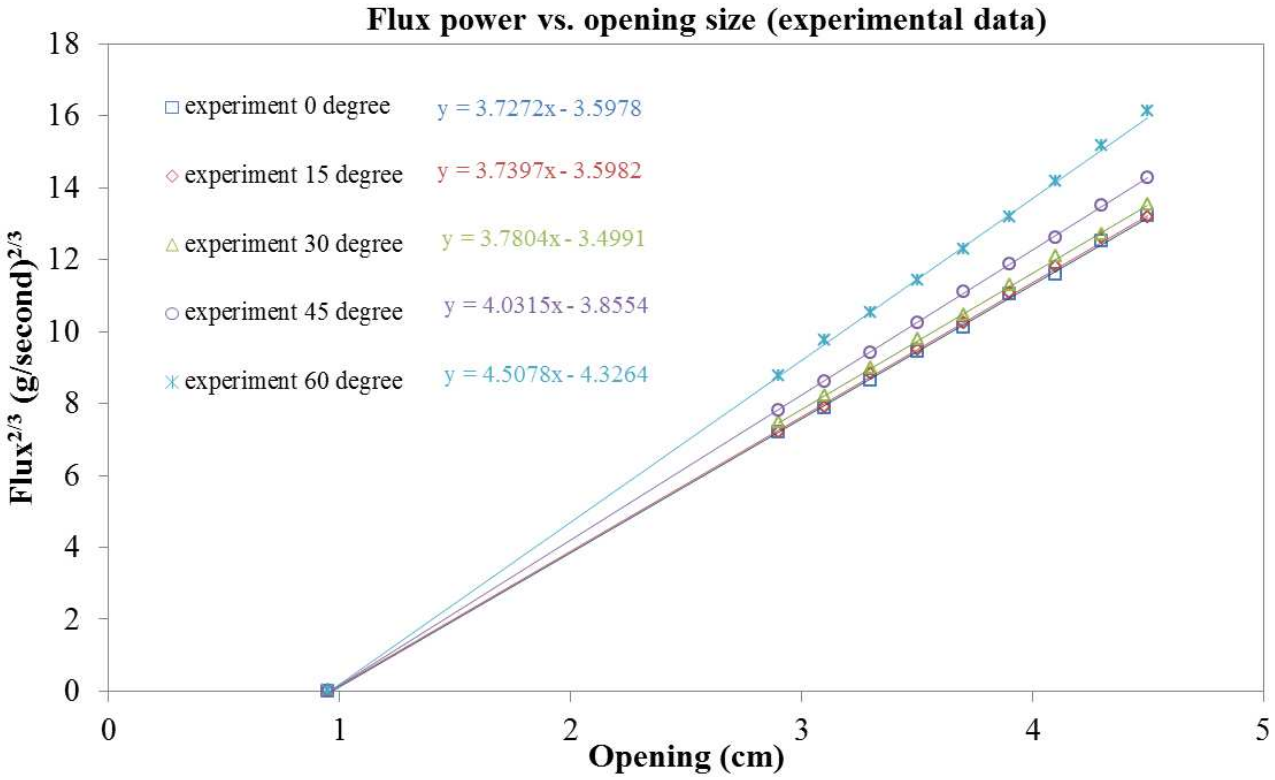

Figure 10: The experimental results for the hopper mass flux.

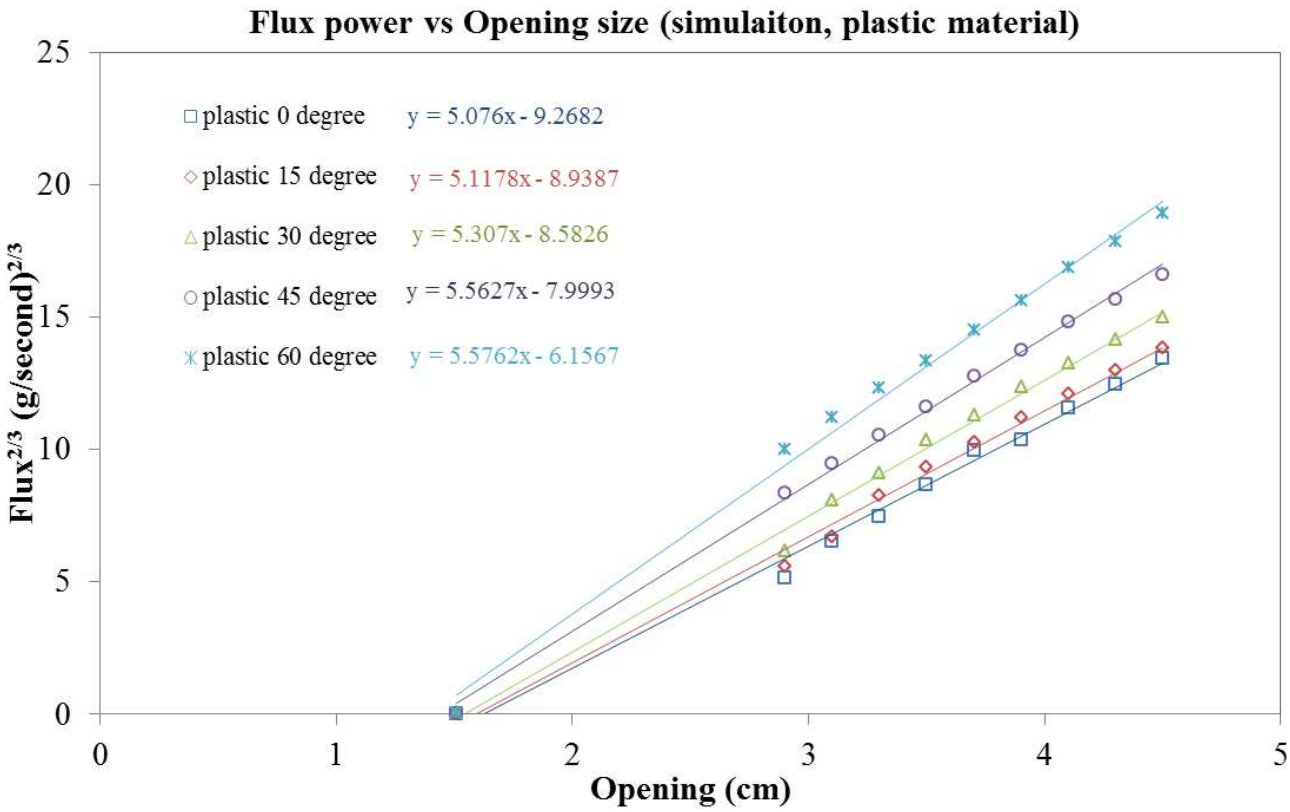

Figure 11: The computational results for plastic material for the hopper mass flux.

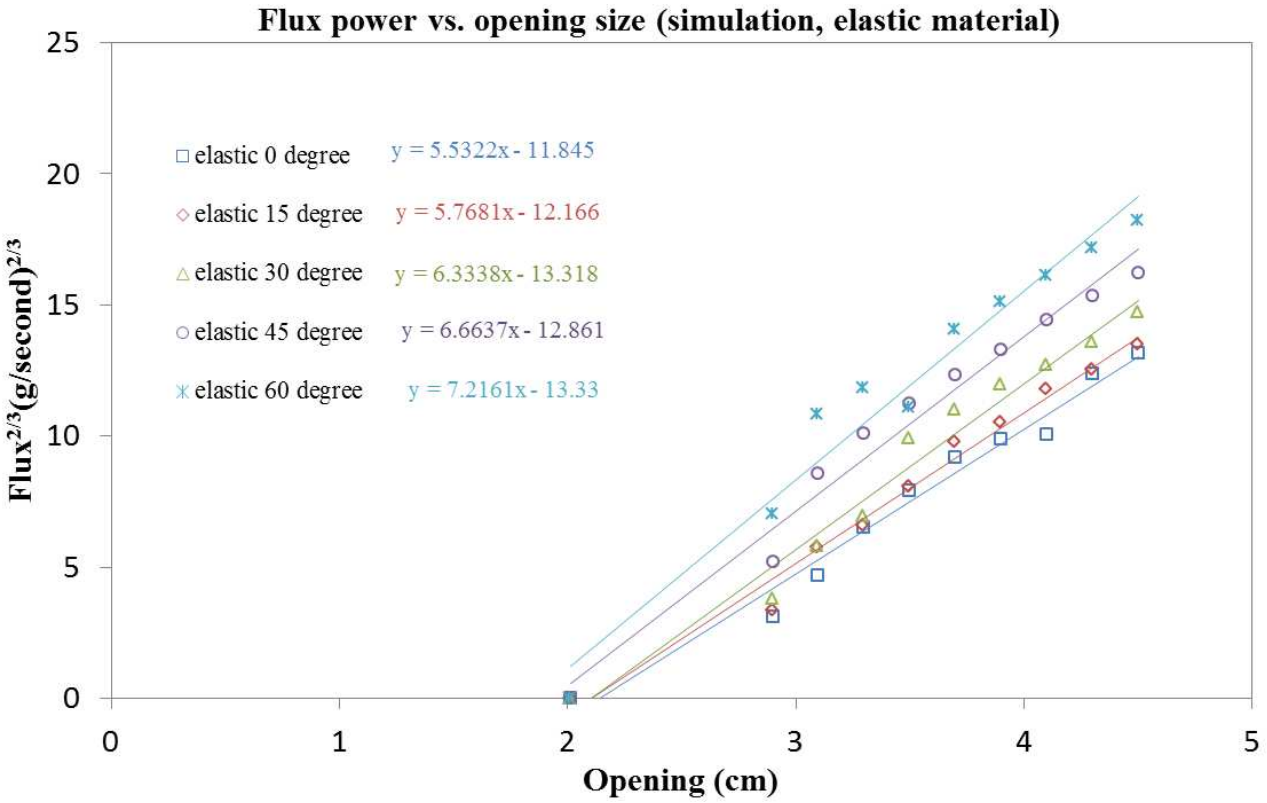

Figure 12: The computational results for elastic material for the hopper mass flux.

the beginning of this section, giving every particle a velocity "kick" and thus letting them flow again can remove the jam. Whenever a jam occurs, the time is recorded, so that we can evaluate the time between jams. With the assumption (cite needed) that the remaining amount of particles in the hopper does not affect the probability of the occurrence of another jam, the time interval between two successive jams is indicative of the survival time of a flow that is newly initiated. Within the twenty multiple simulations, 107 jams occurred in total. In order to build a probabilistic model, we "bin" these inter-jam time intervals in order to obtain a distribution of the likelihood of the jams occurring during each time interval.

The probability that the particle flow in a 2D hopper does not suffer from jamming until time t (i.e., the "survival time") can be calculated according to classical probability, which is validated by the Poisson nature of the jamming events. In order to obtain a useful probabilistic distribution, we add the number of the jams that have occurred in a given "bin" to the number of jams that have happened later than the time corresponding to the "bin", and divide by the total numbers of jams. For example, if we imagine a bin that corresponds to a very short time, there might be no jams that had occurred during that "window".

If we take that "zero" and add to it all of the *later* jams that occur, we get that the probability that the flow will "survive" this time is 1. As we examine a later bin, we similarly compare the current and future jams to the total jams in order to see how likely it is that our flow survives until this time.

The figure 13 shows the probability of survival against time. This is a typical probability distribution function, that the flow is initiated at $t = 0$ and survives until time t, in a similar fashion to what is obtained in the experiment. As with the experiments, this probability $P_s(t)$ is described very well by a decaying exponential with time constant τ, which is denoted

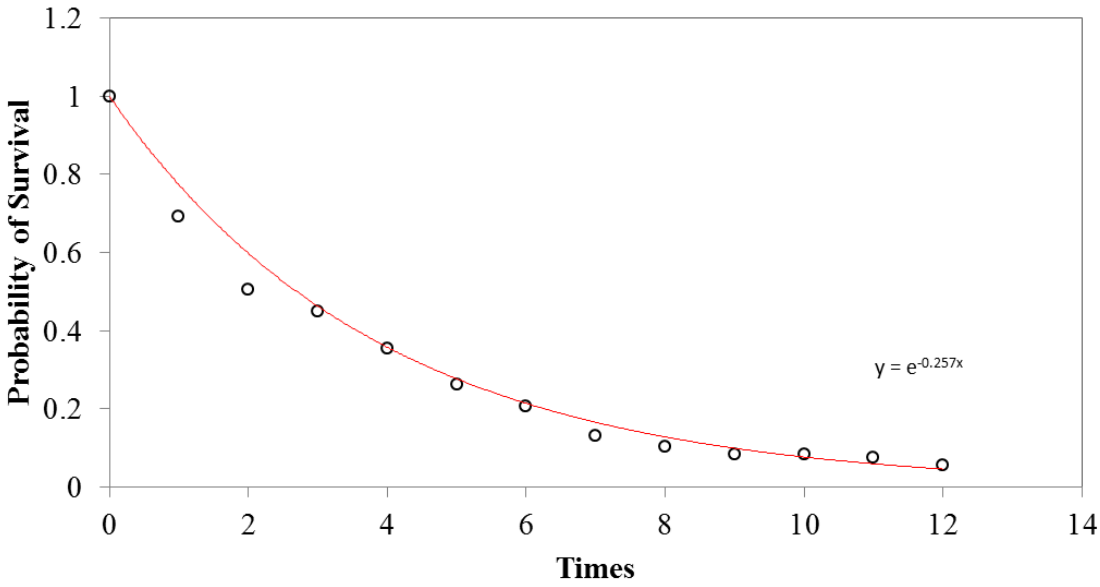

Figure 13: Probability that the flow of particles in the 2D hopper survives until time t obtained by DEM simulation. The red solid line is a fit to a decaying exponential with time constant τ.

as the survival time. Using this probability of survival vs. time plot, the survival time τ can be calculated by $P_s(t) = \exp(-t/\tau)$.

If jamming happens a sufficiently large number of times, the probability plot shown above can be generated. The more times a jam occurs, the more accurate the probability curve will be. Moreover, the better the probability equation is fitted, the more accurate the survival time could be obtained.

In Duke University's study, the survival time was averaged for each hopper opening size among three different angles which include 30°, 45°, and 60°. Nevertheless, the fitting curves for each angle are not very alike. Furthermore, as shown in figure 14, the two experimental curves for 30° and 45° angle respectively in green and purple describe that the coefficient for the bigger angle is a little bit more than the smaller one.

Our simulation yielded enough jams to obtain survival times, τ, only for 15° and 30° hopper angle and the plots for these two angles are shown in figure 14. This is the results for the plastic material since the previous discussion gives that this module fit the experiments better than the elastic one. Although the fitting equation is not close to the experimental result compare the 30° hopper angle result, the trends for these two plots follow the same trends of the experimental curves. Additionally, for our computational data, to better fit the curve, a 95% confidence interval has been made. This lower and higher value for the survival time are marked as the red bars on the plots.

Furthermore, to compare the experimental and computational results, figure 15 was plotted. These four points represent 4 different conditions which include 30° hopper angle with opening size 3.1 cm, 30° hopper angle with opening size 3.3 cm, 45° hopper angle with opening size 2.9, and 45° hopper angle with opening size 3.1 cm.

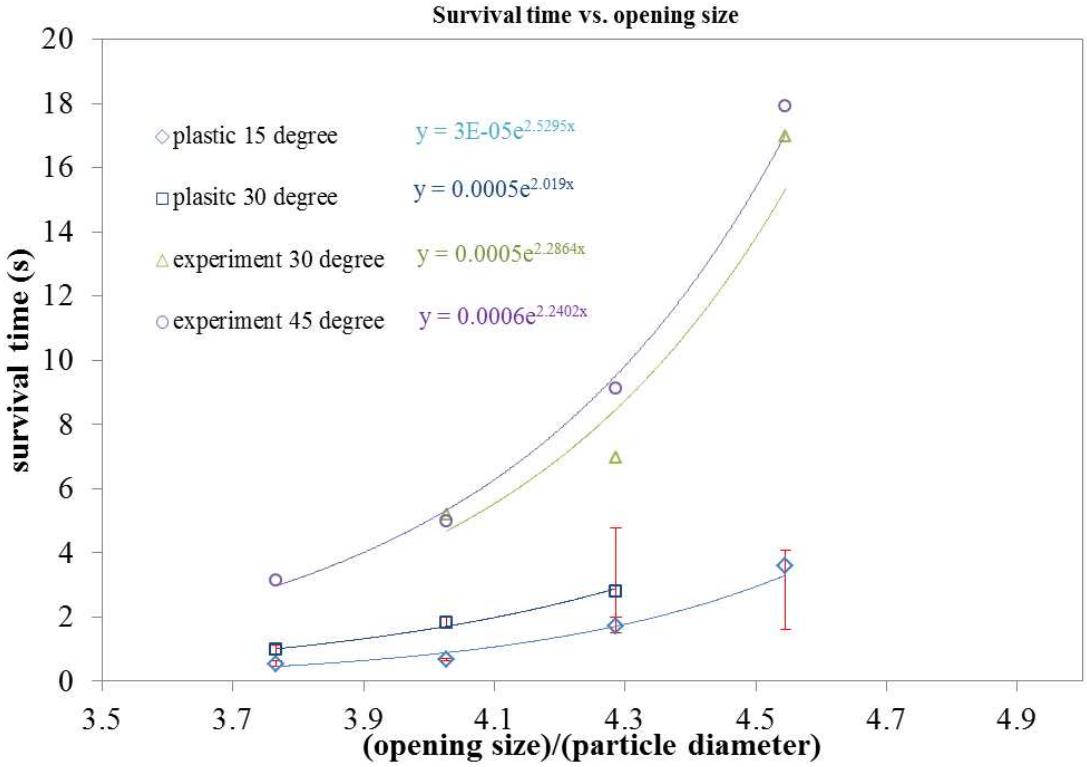

Figure 14: Comparison of experimental(green open triangle and pueple open circle) and computational (red open square and blue open diamond) result for the survival time.

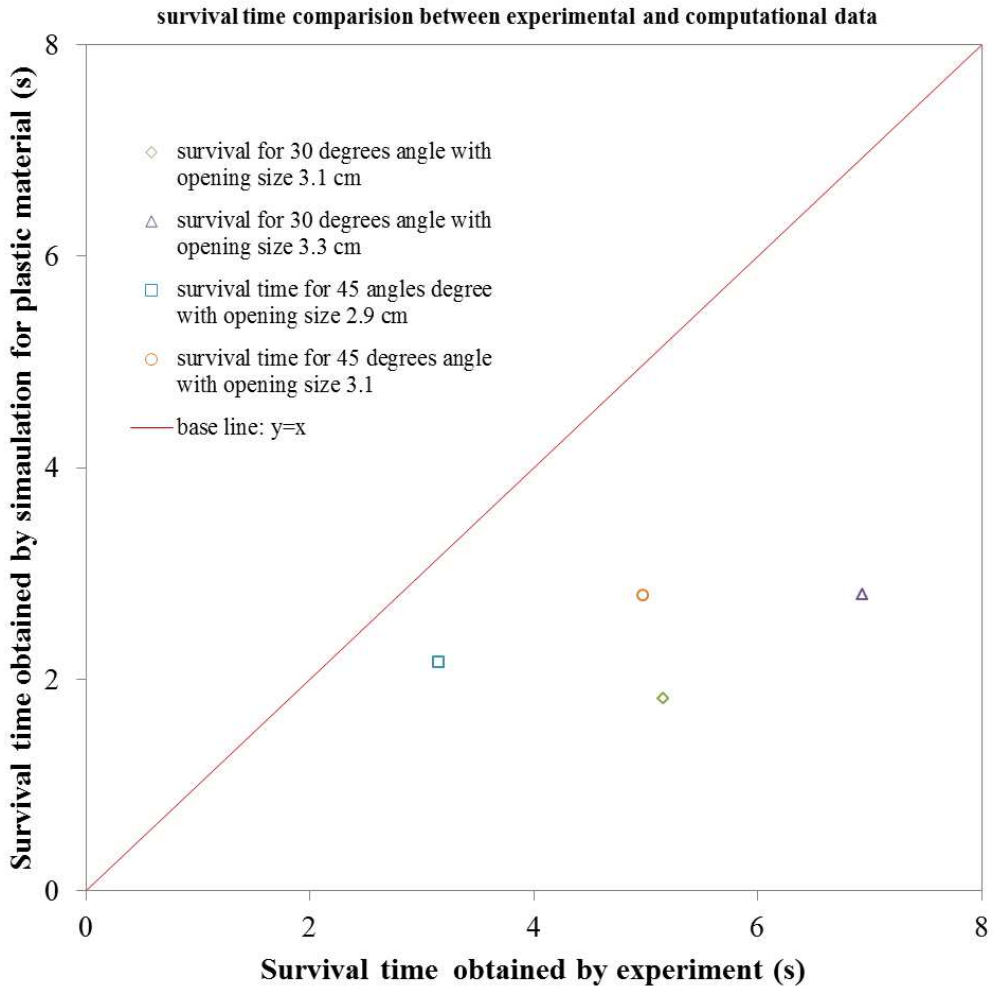

Figure 15: Comparison for survival time τ of experimental and computational result for the plastic material.

If the simulation results match the experimental results perfectly well, all the points should be on the base line as red line shown in figure 15. This figure shows that all the points are below the base line, which means that the survival times obtained in our simulations are all smaller than the ones in the experiments.

5.4 PRESSURE AND VELOCITY PROFILES

In the experiments the high-speed video of the flow was taken with polarizers, while in the simulation we similarly make the pressure profile for the particles in the hopper. Figure 16 [4] and 17 show a jam that has occurred during the course of the flow in the experiment, and in the simulation separately, and depicts the corresponding pressure distribution at the time of the jam. For figure 16, the bright particles are carrying larger forces. Above the hopper outlet, there is a force chain arch that is very clear, which results in the local jamming at the opening.

The same phenomenon can be seen in figure 17. In figure 17, the grey small circles are the particles in the hopper, and the red markings between these particles represent the force between them, which can also be interpreted as the pressure. There is also a red arch above the hopper opening, showing that there is high pressure around the hopper outlet that causes the jam. These two profiles further verify that the DEM simulations can get the results that correspond to the experiments reasonably well.

Figure 18 [4] and 19 shows the velocity profile for the experiments and the simulation separately. For the experiments a sequence of frames for the local particle velocities have been shown in Figure 18. The velocities of the particles become bigger and bigger as they

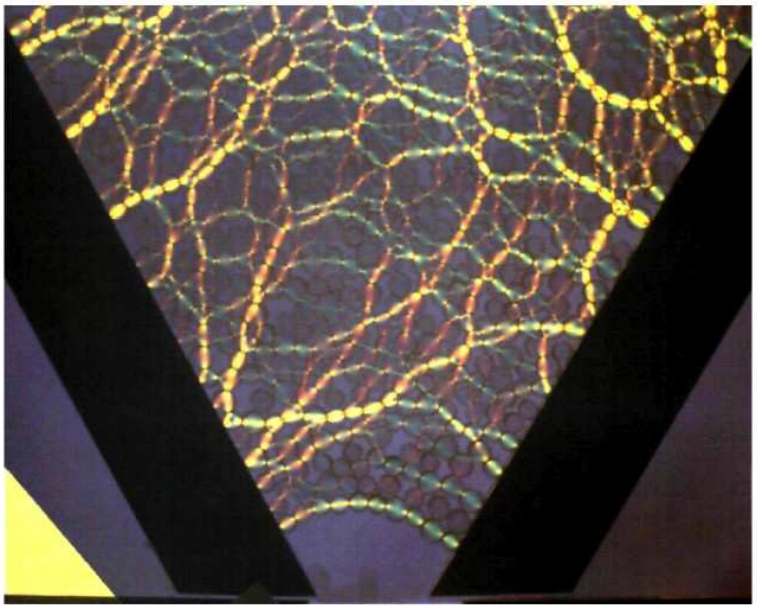

Figure 16: Image showing photoelastic particles between crossed polarizers. Evident is a strong force chain at the outlet which is supporting grains immediately above. Note: used by permission

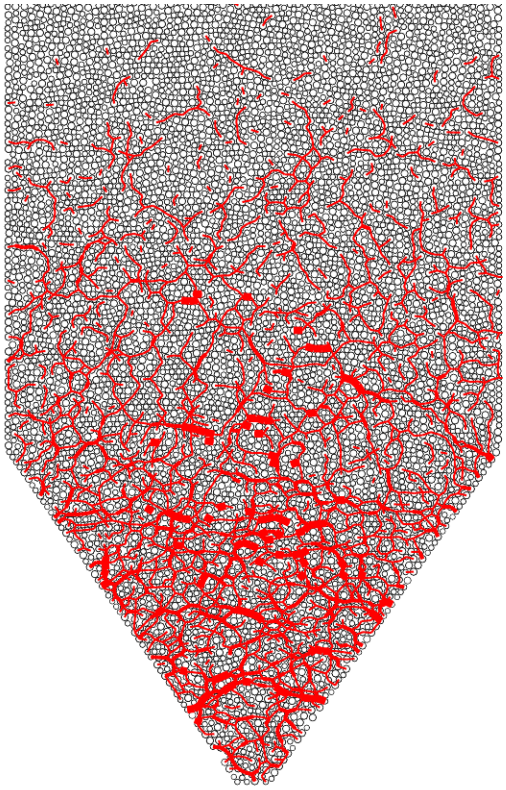

Figure 17: Particle normal stress profile for the 60 degree hopper by DEM simulation

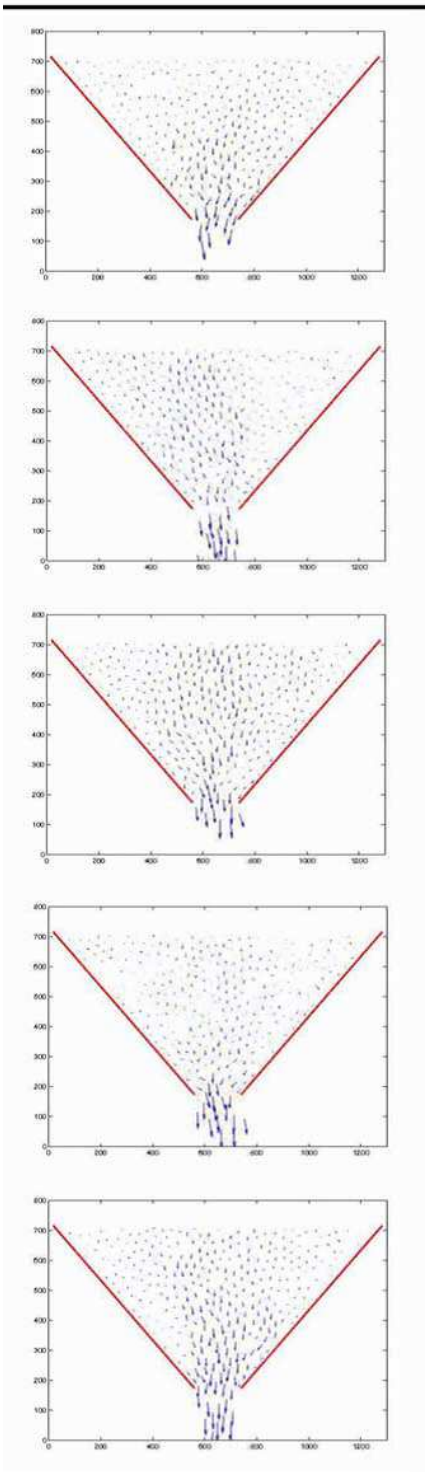

Figure 18: sequence of images, from top to bottom, shoing the local flow velocities of particles. Note: used by permission

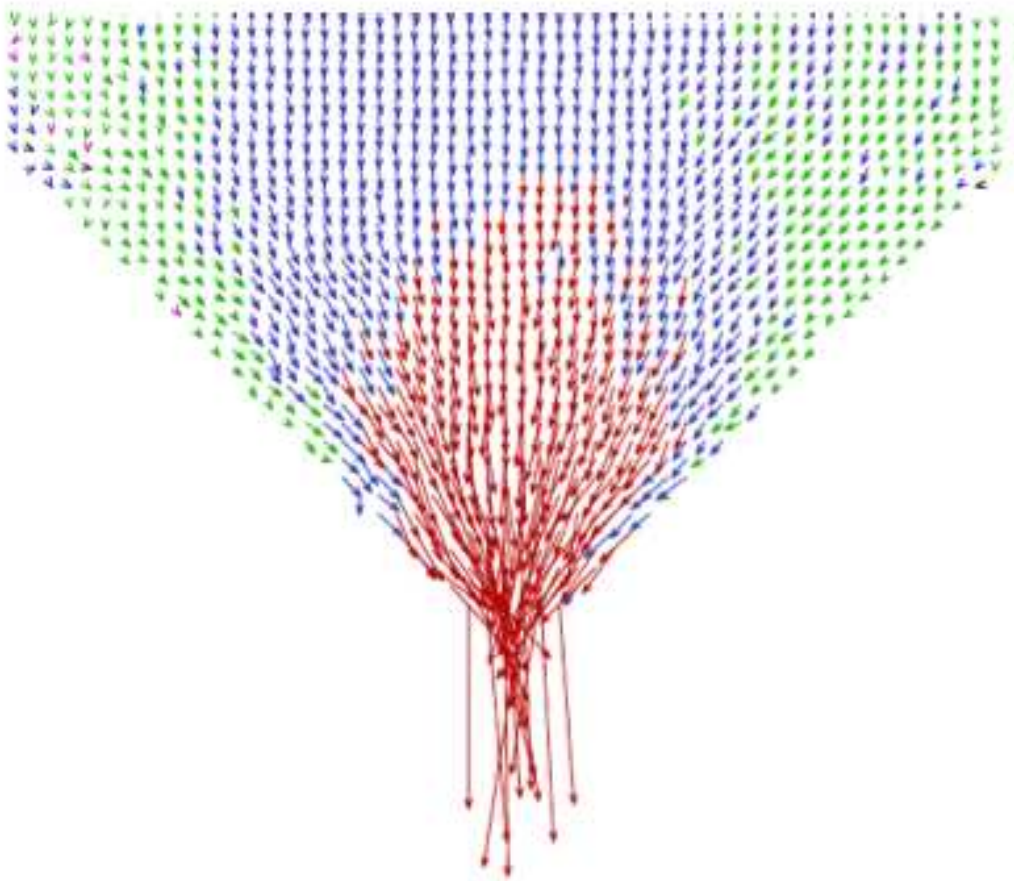

Figure 19: Velocity profile for the 45 degree hopper by DEM simulation

are close to the hopper outlet. In the simulation, we also plot the profile of the particles' velocities as presented in figure 19. Six different colors have been used to describe the magnitude of the particles' velocities. From smaller than 0.003 m/s to bigger than 0.1 m/s, the colors are black, blue, purple, green, light blue, and red respectively. Additionally, the length of the arrows also stands for the velocity value. In accordance with the frame obtained by the experimental data, in the simulation figure, the velocities are their largest around the hopper outlet as well.

6.0 CONCLUSION AND OUTLOOK

This work employs the discrete element method to model the discharge of granular materials from a 2D hopper with different opening sizes and hopper angles. Since well-simulated results are obtained in most aspects, such as the pressure profile, the velocity profile, the prediction of the probability of jamming, DEM simulation of the granular materials from hopper could be a very promising application in the engineering industries. However, the hopper empty times, especially for the elastic model and the smaller hopper opening sizes, might need to be reconsidered if it is required that we obtain better matching. The deviation generated in the empty time results between our simulation and the experiment could be due to the differences in particle shape and the size distributions of the materials. It should be note again that spheroid particles were used in our simulation, rather than the cylindrical ones in the experiments. The proper choice of normal dissipation mode for this material appears to be a plastic model from these results.

In terms of model refinement, data could be refit to a wider dynamic range of experimental values to improve the model's performance in matching the empty time and perhaps the flux trends. To further match the experiment, cylindrical models could be explored as opposed to spheres. Another option would be to do model fitting on a per-particle basis rather than using a collective basis. In this case, a drop tests for single particle validation

can be incorporated. The drop tests use a vacuum release technique to drop particles in a draft-proof tower onto plates of the same bulk material. The initial height of the drops can be varied to bracket the range of impact velocities relevant to the apparatus of interest and high-speed video can be used to extract the coefficient of restitution from the experiments. Finally, it would be of interest to ascertain the surface energy of the particles in order to determine whether adhesive modeling should be included.

BIBLIOGRAPHY

[1] Anshu Anand, Jennifer S. Curtis, Carl R. Wassgren, Bruno C. Hancock, and William R. Ketterhagen. Predicting discharge dynamics from a rectangular hopper using the discrete element method (dem). *Chemical Engineering Science*, 63(24):5821 – 5830, 2008.

[2] B. J. Ennis, J. Green, and R. Davies. The legacy of neglect. *Chemical Engineering Progress*, April:32–43, 1997.

[3] R.M. Nedderman, U. Tüzün, S.B. Savage, and G.T. Houlsby. The flow of granular materials—i: Discharge rates from hoppers. *Chemical Engineering Science*, 37(11):1597 – 1609, 1982.

[4] Sepher Sagdiphour Junyao Tang and R.P. Behringer. Jamming and flow in 2d hoppers. *POWDERS AND GRAINS 2009: PROCEEDINGS OF THE 6TH INTERNATIONAL CONFERENCE ON MICROMECHANICS OF GRANULAR MEDIA*, 1145, 2009.

[5] A.W. Jenike. Quantitative design of mass-flow bins. *Powder technology*, 76(3):237–244, 1967.

[6] G. Enstad. On the theory of arching in mass flow hoppers. *Chemical Engineering Science*, 30(10):1273 – 1283, 1975.

[7] J. C. Williams. The rate of discharge of coarse granular materials from conical mass flow hoppers. *Chemical Engineering Science*, 32:247–255, 1977.

[8] Bates L. McGee E., Marjanovic P. Improving flow from hoppers using inserts and novel wall profiles. *Proceedings of the Seventh International Conference on Bulk Materials Storage, Handing and Transportation*, 1:103–122, 2001.

[9] Manbeck H B Hogg R Kamath S, Puri V M. Flow properities of powders using four testers-measurement, comparison and assessment. *Powder Technology*, 76:3, 277-289 1993.

[10] R. Arévalo, A. Garcimartín, and D. Maza. A non-standard statistical approach to the silo discharge. *The European Physical Journal - Special Topics*, 143(1):191–197, 2007.

[11] J. Schäfer, S. Dippel, and E. Wolf. Force schemes in simulations of granular materials. *J. Phys. I*, 67:1751–1776, 1991.

[12] J. J. McCarthy, V. Jasti, M. Marinack, and C. F. Higgs. Quantitative validation of the discrete element method using an annular shear cell. *Powder Technology*, 203(1):70–77, 10 2010.

[13] P. A. Cundall and O. D. L. Strack. A discrete numerical model for granular assemblies. *Géotechnique*, 29:47–65, 1979.

[14] J. J. McCarthy and J. M. Ottino. Particle dynamics simulation: A hybrid technique applied to granular mixing. *Powder Technology*, 97:91–99, 1998.

[15] C. S. Campbell and C. E. Brennen. Chute flows of granular material: some computer simulations. *Journal of Applied Mechanics*, 52:172–178, 1985.

[16] Y. Tsuji, T. Tanaka, and T. Ishida. Lagrangian numerical simulation of plug flow of cohesionless particles in a horizontal pipe. *Powder Technology*, 71:239–250, 1992.

[17] K. Z. Y. Yen and T. K. Chaki. A dynamic simulation of particle rearrangement in powder packings with realistic interactions. *Journal of Applied Physics*, 71:3164–3173, 1992.

[18] S. T. Nase, W. L. Vargas, A. A. Abatan, and J. J. McCarthy. Discrete characterization tools for wet granular media. *Powder Technol.*, 116:214–223, 2001.

[19] C. Thornton and Z. Ning. A theoretical model for the stick/bounce behavior of adhesive, elastic-plastic spheres. *Powder Technology*, 99:154–162, 1998.

[20] K. L. Johnson. *Contact Mechanics*. Cambridge University Press, Cambridge, 1987.

[21] J. T. Oden and J. A. C. Martins. Models and computational methods for dynamic friction phenomena. *Computer Methods in Applied Mechanics and Engineering*, 52(1-3):527–634, 1985/9.

[22] C. Thornton and C. W. Randall. Applications of theoretical contact mechanics to solid particle system simulation. In M. Satake and J. T. Jenkins, editors, *Micromechanics of Granular Material*, pages 133–142. Elsevier Science Publishers, Amsterdam, 1988.

[23] C. Mankoc, A. Janda, R. Arévalo, J. Pastor, I. Zuriguel, A. Garcimartín, and D. Maza. The flow rate of granular materials through an orifice. *Granular Matter*, 9(6):407–414, 2007.

[24] F.C. Franklin and L.N. Johanson. Flow of granular material through a circular orifice. *Chemical Engineering Science*, 4(3):119 – 129, 1955.

[25] J.C Brown R.L., Richards. Profile of flow of granules through apertures. *Transactions of the Institution of Chemical Engineers*, 38:243–250, 1960.

[26] W.A. Beverloo, H.A. Leniger, and J. van de Velde. The flow of granular solids through orifices. *Chemical Engineering Science*, 15(3–4):260 – 269, 1961.

[27] B.J. Crewdson, A.L. Ormond, and R.M. Nedderman. Air-impeded discharge of fine particles from a hopper. *Powder Technology*, 16(2):197 – 207, 1977.

[28] Hans Peter Kurz and Hans Rumpf. Flow processes in aerated silos. *Powder Technology*, 11(2):147 – 156, 1975.

[29] D.M. Walker. An approximate theory for pressures and arching in hoppers. *Chemical Engineering Science*, 21(11):975 – 997, 1966.

[30] Akke S. J. Suiker and Norman A. Fleck. Frictional collapse of granular assemblies. *Journal of Applied Mechanics*, 71(3):350, 2004.

[31] Jiyu Zhang and Victor Rudolph. Effect of shear friction on solid flow through an orifice. *Industrial & Engineering Chemistry Research*, 30(8):1977–1981, August 1991.

[32] Richards J.C. Brown R.L. Kinematics of the flow of dry powders and bulk solids. *Rheologica Acta*, 4:153, 1965.

[33] R. L. Brown and J. C. Richards. *Principles of Powder Mechanics*. Pergamon Press, Oxford, 1970.

[34] Tanaka T. Rose H.E. Rate of discharge of granular materials from bins and hoppers. *Engineer*, 208:465–469, 1959.

[35] Hector Pacheco-Martinez, Henk J. van Gerner, and J. C. Ruiz-Suarez. Storage and discharge of a granular fluid. *Physical Review E (Statistical, Nonlinear, and Soft Matter Physics)*, 77(2):APS—6, 2007.

[36] Iker Zuriguel, Luis A. Pugnaloni, Angel Garcimartin, and Diego Maza. Jamming during the discharge of grains from a silo described as a percolating transition. *Phys. Rev. E*, 68(4):030301, SEP 2003.

[37] Iker Zuriguel, Angel Garcimartin, Diego Maza, Luis A. Pugnaloni, and J. M. Pastor. Jamming during the discharge of granular matter from a silo. *Phys. Rev. E*, 71(9):051303, May 2005.